Materials & Design 266 (2026) 116243

Contents lists available at ScienceDirect

Materials & Design

journal homepage: www.elsevier.com/locate/matdes

Structural adhesive bonding between layers in additive manufacturing composites

Magdalena Mieloszyk [a,*], Marius Rimasauskas [b], Suvam Bhadra [a], Muhammad Abuzar Khan [a,b]

[a] Institute of Fluid-Flow Machinery, Polish Academy of Sciences, Fiszera 14, 80-231 Gdansk, Poland
[b] Kaunas University of Technology, Studentu 56, Kaunas 51424, Lithuania

ARTICLE INFO

Keywords:
Additive manufacturing
Structural integrity
Temperature
THz spectroscopy
Fibre/ polymer bonding
Adhesive joint

ABSTRACT

In additive manufacturing (AM) structures, the quality of adhesive bonding between consecutive printing lines and layers is crucial for the structural integrity and mechanical performance of the manufactured elements. This paper analyzes the quality of adhesive bonding in AM carbon fiber-reinforced polymer (CFRP) produced using a modified material extrusion process (MEX) developed by Kaunas University of Technology. The modification replaces two separate printing heads (for polymer and fiber filaments) with a single head to enhance structural integrity through improved interlayer adhesion, and it also introduces a dedicated fiber preparation procedure prior to printing that affects adhesive bonding quality. Scanning electron microscopy and terahertz spectroscopy were used to evaluate the composites both immediately after manufacturing and after exposure to temperature variations (elevated and sub-zero), and tensile testing was performed on the samples. The analyses focused on the quality of adhesive bonding between printing lines (impregnated carbon fibers) and consecutive layers. The results show that the pre-impregnation process substantially improves the quality of the adhesive joint between the fiber and the matrix. In addition, two polymer types were identified in the AM-produced CFRP: the first, originating from pre-impregnation, covers the carbon fiber, while the second originates from the 3D printing process.

1. Introduction

Additive manufacturing (AM) methods have recently gained popularity due to ecological advantages, such as the ability to produce components with complex geometries while generating minimal waste, and they can be applied to a wide range of materials, including polymers, metals, and ceramics; these benefits have contributed to their growing adoption across various industries. Among AM approaches, one method applicable to the manufacturing of both pure polymer and fiber-reinforced polymer (FRP) elements is based on the material extrusion process (MEX), which, owing to its simplicity and the lack of need for support material, remains one of the most widely used AM methods. MEX has also emerged as a particularly prominent approach for composite fabrication because it can accommodate high fiber loadings and can even enable the use of continuous fiber reinforcements through specially designed filaments or dual-nozzle systems [1]. This makes MEX an attractive method for printing FRP components. However, despite these advantages, MEX introduces specific challenges related to the resulting material microstructure and the quality of interfacial bonding.

The 3D-printer for the standard MEX method contains one or two separated nozzles: one for thermoplastic polymer and the second for fibre reinforcement[2]. Both components are in the form of flexible filaments. The final element is created on a heated build platform. During the 3D-printing process, due to heating inside the printing head, the polymer is gradually softened and melted. Both materials (polymer and fibre) are subsequently extruded through nozzles onto the building platform. The process is continued until manufacturing the final product [3].

The modification proposed by the Kaunas University of Technology is related to design a new solution of a printing head with one nozzle for both materials: polymer and continuous fibre reinforcement. The purpose of such modification was to increase the adhesion between fibre and matrix. The 3D-printer modification is linked with pre-impregnation process of fibre reinforcement with the same polymer used then during

* Corresponding author.
E-mail address: mmieloszyk@imp.gda.pl (M. Mieloszyk).

https://doi.org/10.1016/j.matdes.2026.116243
Received 7 November 2025; Received in revised form 5 May 2026; Accepted 15 May 2026
Available online 15 May 2026

the AM. This approach led to better adhesion between neighbouring impregnated fibre reinforcements in the final element. The thickness of one layer depends on the diameter of the continuous fibre reinforcement bundle, however for better quality of structure, the layer thickness should be as small as possible. The principle of operation of the method is reported in detail in the paper [4].

The AM process results in the accumulation of residual stresses due to the polymer's rapid contraction during its transition from one physical state to another. Problems in adhesion between printed fibres results in voids occurrence that decrease the mechanical strength of FRP material [5]. The other weak points are the bonds between fibres and the matrix. Degradation processes in this area result in decreasing the mechanical strength of the whole FRP element[6]. However, investigating degradation models is complicated because commercially available short carbon fiber-reinforced thermoplastics contain various additives like stabilizers and plasticizers [7].

In contrast to the standard manufacturing technique, the mMEX method inherently fabricates components through successive layering without applying external consolidation forces, presenting a significant obstacle to achieving good interlayer adhesion. The interfaces between deposited layers are often weaker than the bulk material within each layer, which aggravates the strength and toughness in the build direction and can compromise the overall functionality of the fabricated part [8,9]. In traditional composite manufacturing (e.g. lay-up with autoclave curing or compression moulding), substantial pressure and controlled curing are applied to ensure near-void-free consolidation and robust interlaminar bonds. However, additively manufactured CFRP parts typically exhibit relatively poor interlaminar bonding and higher void content compared to their conventionally manufactured counterparts. To improve interfacial shear strength, carbon fibres can be dip-coated in the suspension of nanotubes [10]. The lack of pressure during MEX means that the deposited paths of melted polymer are not fully pressed together, often resulting in incomplete diffusion at the layer interface. As a result, micro-voids and weak filament-to-filament contacts remain in the structure. These interlayer defects directly translate into inferior through-thickness mechanical properties: additively manufactured CFRP components tend to exhibit substantially lower strength and stiffness in the *Z*-direction and are prone to delamination or fibre pull-out under loading, unlike the well-consolidated laminates made by traditional methods[11]. This disparity underscores the need for closer observation of interlayer adhesion in AM composites, as it is a key factor limiting their performance.

Due to their widespread application, FRP materials are often exposed to diverse environmental conditions. Among these, temperature is one of the most critical factors influencing both the overall material durability and integrity of the adhesive joints in the AM FRP material. This sensitivity arises from the heterogeneous nature of the FRP materials, which comprise constituents with distinct mechanical and thermal properties. Temperature changes strongly influence polymer and polymer/fibre (matrix/reinforcement) bonds. Both elevated and sub-zero temperatures affect polymer matrix chemical and physical properties, resulting in matrix cracking, plasticisation, crystallisation, etc. [12–15]. Elevated temperatures have been shown to reduce adhesion at the reinforcement-matrix interface[12,13]. Sub-zero temperatures adversely affect the fibre–matrix bond, primarily due to damage-inducing stresses arising from the mismatch in the thermal expansion coefficients of the fibres and the polymer resin[16]and local phase change (from amorphous to crystalline structure) of the polymer.

The paper is organized as follows. First, the manufacturing method and the samples used are presented. Three types of samples are analysed: fibre with polymer disc, composite samples in the form of laminates and adhesive joints between two laminates. The samples are tested using a destructive method (tensile test) and two structural analysis methods: scanning electron microscopy (SEM) and terahertz (THz) spectroscopy. The analyses focus on adhesive joints between the polymer and the fibre. The presented tests start from the base connection (between polymer and impregnated or non-impregnated carbon fibre). Results show that the pre-impregnation process strongly increases the quality of the adhesive connection. Then, composite samples are manufactured, and the analyses are focused on adhesive joints between fibres and polymers in one layer and between layers. Two polymer types are determined. They originated from two different processes in the additive manufacturing method. The first comes from the pre-impregnation process, while the second comes from a 3D-printing process. It is observed that in a laminate structure, the quality of adhesive joints between those two polymers is crucial to achieve the mechanical strength. Then, the samples were exposed to sub-zero and elevated temperatures to analyse the influences of temperature on the internal structure. The two polymer types mentioned above can still be determined. Also, adhesive joints between two laminates are analysed to determine their shear strength. Finally, the conclusions are presented.

2. Manufacturing methods and samples

Adhesive joints in additive manufacturing (AM) structures were analysed using two types of samples. The first group consisted of continuous carbon fibre (CCF) and polylactic acid (PLA). The primary objective of these analyses was to evaluate the adhesive joint between the fibre and the polymer, the fundamental joint in AM structures, whose quality determines the mechanical strength of the entire AM element. The second group comprised additively manufactured structures fabricated using the modified material extrusion (mMEX) method and was subsequently exposed to varying temperatures. These analyses aimed to assess the influence of temperature on the internal structure of the AM material. In addition, the quality of adhesive joints formed between two 3D-printed samples was also investigated.

The PLA impregnated CCF tow was produced using a solution-based impregnation technique. A study presents designed and developed an impregnation setup for the impregnation of 1 K and 3 K CCF with PLA polymer[4]. The designations 1 K and 3 K refer to the number of individual carbon filaments contained within a bundle, with 1 K corresponding to 1000 filaments and 3 K to 3000 filaments. The impregnation process involved passing a CCF tow through a solution of PLA pellets dissolved in methylene dichloride. The tow entered the impregnation zone through an input nozzle, passed through the PLA solution, and subsequently exited through an output nozzle. The nozzle's function was to remove excess polymer attached to the tow and mold the tow into the circular filament form. The impregnated CCF tow was directed into the heating chamber, where a hot blast of air (220°C) dried up the impregnated tow before it was wound on the spool, forming impregnated carbon fiber (iCF). The impregnation process was controlled by a stepper motor attached to the winding spool. The speed of the motor determines the impregnation quality. Lower motor speeds allows to have longer contact time between the fibre and the solution, allowing for full fibre wetting and better impregnation quality. In this study, CCF tow T300B-3000 (from Toray) was impregnated with 10% PLA solution. PLA 3D850 biopolymer from NatureWorks and a solvent methylene chloride (CH2Cl2) form Eurochemicals were used to prepare solutions for the impregnation process.

The material extrusion-based MEX printer MeCreator 2 from Geeetech, China, was chosen to print the composite specimens. The printer was modified to print the composite specimen consisting of PLA matrix material and impregnated CCF as a reinforcing agent. It used a dual-input extrusion head. In one input of the extruder, the pre-preg CCF filament was inserted, while in the other input, the standard PLA filament was inserted. The two filaments were melted in the heating zone before being deposited on the printing bed. The operational principle of the modified MEX method is presented in Fig. 1 (a).

The method was used for manufacturing three types of samples: 2-layer laminates, 4-layer laminates and single lap joint (SLJ) specimens. Commercially available Polylite PLA Natural filament with a diameter 1.75 mm was used as the matrix material for sample

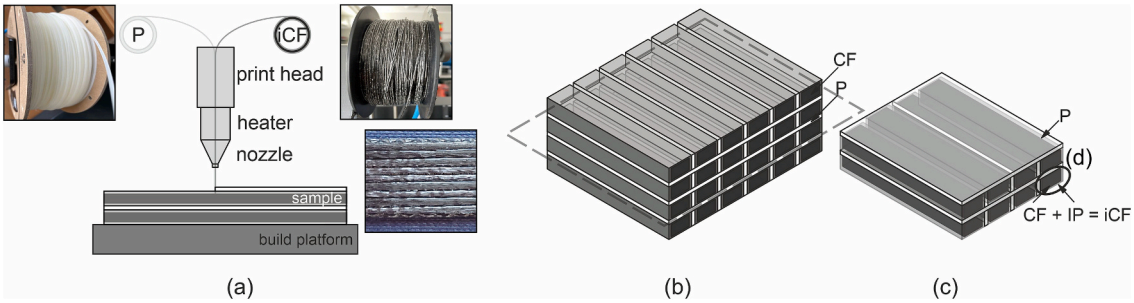

Fig. 1. Modified FDM: (a) printing principle and schema of (b) the 4-layer additively manufactured composite structure, (c) a part of the structure with marked (d) structure of impregnated continuous fibre (iCF); P – polymer, iP – polymer layer on continuous fibre (CF).

production. Meanwhile, non-twisted continuous carbon fiber tow T300B-3000 from Toray was used to prepare specimens for adhesion testing and for single lap joint tests. The printer settings adopted for printing the composite specimen are presented in Table 1.

The 2-layer samples (150 x 15 x 1 mm) were used for the presentation of the internal structure of a laminate using THz spectroscopy method. The structural analyses of samples after manufacturing and after exposure to temperature were performed on 4-layer unidirectional samples with dimensions 150 x 15 x 2 mm. For the determination of interlayer adhesion, it was decided to produce single lap joint specimens. The dimensions of the printed specimens were 130 x 10 x 4 mm. The length of the overlapping joint was 15 mm. To ensure the applied load coincides with the longitudinal axis of the SLJ test specimen, they must be properly aligned in the machine grips. In this study, tabs were fabricated using a material-extrusion-based additive manufacturing process from PLA thermoplastic and bonded to the specimens with ethyl-2-cyanoacrylate adhesive. Prior to bonding, all plastic deposits were removed, and the contact surfaces were prepared to ensure optimal adhesion between the tabs and the samples.

The schema of the carbon fibre-reinforced polymer (CFRP) structure manufactured using the modified MEX method is presented in Fig. 1(b), (c). The schematic presentation assumes that fibres in consecutive layers are printed in parallel in stacks. During the printing process, pre-impregnated continuous fibres (iCF) and continuous fibre (CF) tow, covered by thermoplastic polymer (iP), were used (Fig. 1(c),(d)). The same thermoplastic polymer (P), was used during the AM process. Polymer fills the gaps between iCF and forms a polymeric layer between consecutive layers in the FRP laminate. The adhesive joints between two polymer sets (P and iP) play a crucial role in the mechanical properties of the final element. It is important to notice that it is the same polymer material but placed in the final structure during two different processes (pre-impregnation process and AM). Used procedures also influenced the final structure of the polymer in the additively manufactured sample. The AM process results in the accumulation of residual stresses due to the polymer rapid contraction during its transition from one physical state to another. Another problem is voids that form in areas where the polymer P did not fill the areas between printed fibres.

Table 1
Printing process settings for composite specimen.

Printer Settings	Value, Description
Nozzle diameter	1.5 mm, stainless steel
Extruder temperature	220°C
Extruder multiplier	0.8
Build platform temperature	80°C
Printing speed	180 mm/min
Printing direction	Flat
Fiber direction	0° unidirectional
Infill ratio	100%
Infill pattern	Rectilinear

3. Experimental methods

Structural analyses of AM structures were performed using two methods: scanning electron microscopy (SEM) and terahertz (THz) spectroscopy. The objective of these investigations was to assess the quality of adhesive bonding between printing lines (iCF), as this parameter directly influences the mechanical strength of the material. The analyses were performed on CFRP samples both after manufacturing and following exposure to sub-zero and elevated temperatures. Temperature was selected as the primary variable because it represents the most common environmental factor with a significant impact on material structure.

The mechanical strength and parameters were determined using tensile test, pull-out and interlayer adhesion tests performed using the universal Tinus Olsen H25 KT testing machine.

3.1. Scanning electron microscopy

SEM is a high-resolution imaging technique capable of resolving surface and fracture surface morphology at nanometer scales. In CFRP composites, SEM is widely used to examine cross-sections and fracture surfaces after mechanical testing, allowing researchers to identify local failure modes such as fibre pull-out, fibre breakage and interfacial debonding. Secondary electron imaging is typically used to reveal topography and to distinguish between matrix and fibre phases. Since SEM can reveal fine features (reported resolution ≈ 1 nm), it is well suited for analysing micro voids, gaps between printed rasters and other defects that control the quality of adhesive bonding between layers Liu et al. [17]. SEM analysis complements mechanical testing by revealing failure mechanisms that are often not captured by load vs displacement data. For example, fractographic observations of CFRP laminates containing graphene nanoplatelets showed wrinkles on the fibre surfaces, indicating improved wetting and interfacial adhesion[18].[19]investigated interfacial adhesion between TPU and acrylonitrile butadiene styrene (ABS) or acrylonitrile styrene acrylate (ASA) specimens produced via fused filament fabrication (FFF). Lap-shear tests and cross-sectional SEM analyses revealed that when TPU was printed onto ABS/ASA, effective polymer penetration created a continuous, void-free interface. Conversely, ABS/ASA deposition onto TPU resulted in voids and misalignments due to viscosity differences impeding polymer flow. These observations confirm SEM's critical role in assessing how printing parameters and material combinations influence interlayer bonding in additive manufacturing composites.

When evaluating interfacial adhesion in CFRP composites, it is essential to consider not only layer bonding but also the integrity of the thermoplastic impregnation surrounding the carbon fibre reinforcement. Even when the same polymer (PLA) is used for both impregnation and matrix, SEM observations in our work revealed localized adhesion failures at this fibre–matrix interface, especially in areas where the matrix material was absent or failed to wet the fibre surface adequately. Thermoplastic impregnation can be challenging due to the higher

viscosity. Resin impregnation behaviour in carbon fibre thermoplastics can be strongly influenced by processing conditions and fibre matrix surface energy mismatch. SEM analyses revealed that despite even resin distribution, interfacial bonding between the carbon fibres and recycled glycol-modified poly(ethylene terephthalate) (rPETG)matrix remained inadequate, indicating the absence of chemical bonding and reliance solely on physical interactions [20]. Such insights confirm that absolute material compatibility alone does not guarantee improvement in interfacial bonding, localized adhesion deficits at the impregnation interface can still prevail. In the presented SEM observations, the fracture surfaces exhibited distinct features following elevated and sub-zero temperature exposure. The thermally exposed specimens displayed smoother tear patterns, whereas sub-zero specimens revealed brittle, interfacial cracks. The SEM highlighted areas where the polymer matrix was absent. The poorly bonded zones acted as the crack initiation sites and ultimately lead to the failure of the PLA CFRP specimens. These microstructural observations show the critical interplay between thermal history, matrix continuity, and interlayer adhesion in determining the structural performance of MEX printed CFRP.

3.2. Thz spectroscopy

The internal structure of a composite element can be inspected using different non-destructive testing (NDT) methods based on electromagnetic radiation, as it is presented in Fig. 2. THz range of electromagnetic waves is typically from 0.1 THz to 10 THz. The power generated by THz beam (especially pulsed signal) is very low (meV), and the radiation has a non-ionising character. Therefore, it is not dangerous for humans [21]. Imaging process using THz radiation based on changes in THz wave parameters: refractive index, absorption coefficient, or wave scattering [21].

The application of the THz spectroscopy method to inspect the internal structure of an element is limited to non-conductive materials. The THz wave is totally reflected from conductive materials (like metals or carbon fibres), so the method can only be used for the element's surface. Thus, the THz technique can be used for inspection of internal structures, tissues ()[22], paper [23], glass fibre reinforced polymer [24–28], aramide fibre reinforced polymer [29], and sandwich panel with glass fibre reinforced polymer skins and pouliretane core [30]. For materials containing both conductive and non-conductive components the application of THz spectroscopy for the internal structure inspection depends on percentage amount of conductive particles and their distribution [27].

A CFRP material contains conductive carbon fibres and a non-conductive polymeric matrix. In CFRP samples manufactured using standard techniques (e.g. autoclave or infusion method), the application of THz spectroscopy is limited to the detection and localisation of surface damage. It can be related to polymeric coating quality and adhesion to the CFRP surface due to the malfunction of the coating manufacturing process, like missing cleaning steps, contamination, and an improper amount of topcoat [31]. The other types of damage are surface damage of the CFRP element, like burn damage[32]or impact damage. This is due to the fact that carbon fibre content is approximately 60%-70% of the total weight of the laminate. On the contrary, in CFRP samples manufactured using mMEX method, the typical fibre content is 18%-20% of total weight. Therefore, in a unidirectional CFRP laminate, the

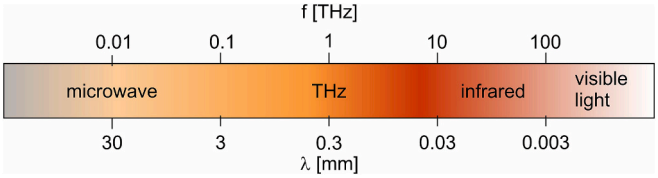

Fig. 2. Electromagnetic wave spectrum with marked THz range.

THz wave can propagate throughout the whole thickness of the element [27] and can be applied for structural analyses of the element.

The used THz spectrometer device was TPS Spectra 300 THz Pulsed Imaging and Spectroscopy from TeraView. It contains both the scanning unit and the measurement chamber, as presented in Fig. 3. The measurement chamber allows the determination of material parameters (e.g. refractive index, absorption coefficient) of the sample. The scanning unit contains a moving platform that allows analysis of the chosen area of a sample in three dimensions (x-, y-, z-axis). The maximal dimension of the examined element in the xy plane is equal to 700 mm x 700 mm. The scanning heads were arranged in a reflection mode in their xy-plane. The angle between the heads was equal to 22°. During the measurements, the samples were placed on a metal table. The table material was chosen to reflect all signals that travelled throughout the entire sample thickness. The measurement step was equal to 0.2 mm in both directions in the xy plane, and the THz signals were recorded with 10 times averaging. The time difference in each measured signal was equal to 0.0632 ps.

The data achieved from THz spectroscopy are presented in the form of the imaging techniques: A-scan, B-scan and C-scan. A-scan is a graph showing a time domain signal measured at one point. The signal shape contains reflections from boundaries between media (e.g. air/polymer). B-scan is a visual representation of a set of A-scan measured along a chosen line. It allows inspection of a chosen cross-section of the analysed sample. Signals collected for all points in the chosen area create a 3D matrix. C-scan is a map presenting signal amplitudes for all points for the chosen time delay.

3.3. Mechanical test Methodology

Two types of mechanical tests were performed related to adhesion analysis. The first was related to adhesion between CCF and polymer, while the second was to interlayer adhesion. Both tests were performed on the universal Tinus Olsen H25 KT testing machine.

Adhesion analysis was conducted on 3 K impregnated and non-impregnated CCF tows. PLA pellets were introduced into a mold specifically designed for adhesion testing. For the impregnated filament, a pellet mass of 0.3 g was used. For the non-impregnated CCF tow, pellet masses of 0.3, 0.5, and 1 g were employed. In the case of the impregnated CCF, a 0.3 g pellet was placed into the mold, through which the tow was passed. The mold was then heated in an oven at 215°C to melt the PLA pellets. After heating, the mold was removed from the oven and allowed to cool to room temperature before being opened. A schematic diagram of a pull-out test is presented in Fig. 4(a), while fabricated specimens are in Fig. 4(b).

A similar procedure was applied to the non-impregnated tow, using pellet masses of 0.3, 0.5, and 1 g. In this case, the mold was heated at 215°C for 10 min, after which it was opened to obtain the samples. Each group of adhesion tests consisted of 10 samples. In total, 40 samples were prepared for adhesion testing, which was carried out using the pull-out technique.

A schematic diagram of the interlayer adhesion testing is presented in Fig. 4(c). The tests were performed on six samples printed utilising the mMEX method. The failure modes were classified according to ASTM D5573.

Fibre pull-out and interlayer adhesion tests were performed using the universal Tinus Olsen H25 KT testing machine, with a 2 mm/min crosshead speed. Tinius Olsen software, Horizon, was used for machine control, data acquisition, and analysis. Tabs at the end of impregnated and non-impregnated carbon fibre were used to create a reliable grip. Tabs were clamped in manual wedge-action grips. The adhesion testing between the matrix material and continuous carbon fibre was performed by using the fibre pull-out procedure. The crosshead of the machine moves upwards, thus creating the tension and the force is recorded until the continuous carbon fibre tow is successfully pulled out or is broken.

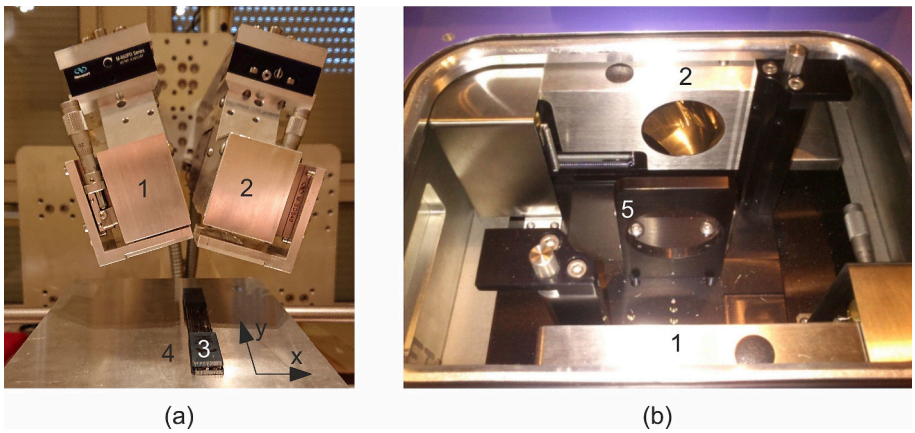

Fig. 3. THz spectrometer: (a) scanning unit in reflection mode, (b) measurement chamber; 1 – emitting head, 2 – receiving head, 3 – CFRP sample, 4 – metal table, 5 – sample holder.

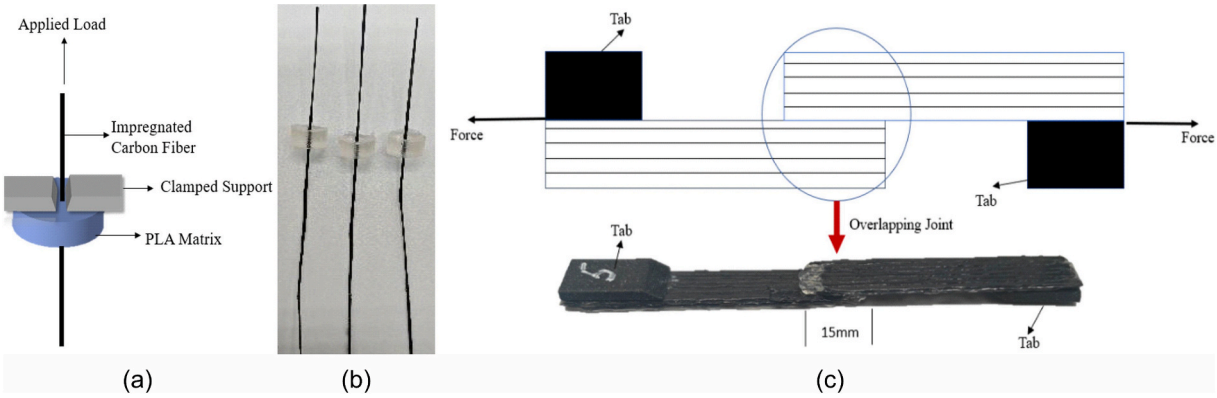

Fig. 4. (a) Schematic diagram of the fibre pull-out test, (b) samples for pull-out testing, (c) schematic diagram and printed composite sample for interlayer adhesion testing.

4. Results and discussion

4.1. Adhesion analysis between CCF and polymer

The adhesion testing between impregnated, non-impregnated CCF tow and polymer matrix was performed using the fibre pull-out procedure. In Fig. 5, the curves show the behaviour of samples from different groups during mechanical testing. The plot reveals a significant increase in the adhesion force for the impregnated tow. The steeper slope corresponds to the higher adhesion forces between the fibre and the polymer. When 0.3 g of PLA polymer was used for the impregnated filament, the adhesion force increased to 127 N. At this load, the fibre breakage was witnessed instead of fibre pull-out. This suggests that the force of adhesion between the impregnated fibre and the polymer is more than the breakage force of the fibre. The 0.3, 0.5 and 1 g of polymer were employed for the non-impregnated tow. The results revealed that increasing the amount of polymer led to a corresponding increase in the adhesion force for the non-impregnated tow. This can be explained by the fact that adding more polymer material increases the contact surface area between the polymer and the carbon fiber; accordingly, the adhesion force increases. The plot in Fig. 5(b) shows a comparison of adhesion force for the impregnated and non-impregnated tow. The force of adhesion for the non-impregnated filament is less than that of the impregnated filament, and the force of adhesion is increased for the non-impregnated filament by increasing the amount of polymer.

4.2. Interlayer adhesion testing results

To determine shear strength, the six SLJ samples were designed and printed utilising the mMEX method. The testing results and single lap joint shear strength, including statistical analysis are provided in Table 2. The shear area for each sample was calculated individually by multiplying the length of the overlapping region by the width of the sample. The shear strength was then determined as the ratio of the maximum force to the corresponding shear area. The curves presented in Fig. 6 show consistent responses and similar mechanical behaviour across all samples. The obtained force values ranged from 936 N to 1280 N for Sample 1 and Sample 6, respectively, while the measured shear strength ranged from 7.4 MPa for Sample 1 to 8.8 MPa for Sample 6. The sudden drop observed after the peak load indicates a brittle fracture mechanism, caused by matrix debonding in the single lap joint region. Despite the fact that there is a significant change in force, in this study shear strength is the most interesting parameter because it normalizes force values against the specific adhesion area of each sample. Overall, the standard deviation associated with the peak-load measurements indicates limited specimen-to-specimen scatter, suggesting consistent interlayer bonding. Furthermore, the coefficient of variation of 6.6% confirms the high reliability and reproducibility of the shear strength results. The average shear strength value is 8.1 MPa with confidence interval 7.5–8.6 MPa. The relatively low scatter in shear strength (coefficient of variation, CV $\approx$ 6–7%) indicates limited specimen-to-specimen variability and suggests stable, reproducible interlayer bonding. The 95% CI for the mean shear strength indicates that the average interlayer adhesion strength is estimated for n = 6, consistent

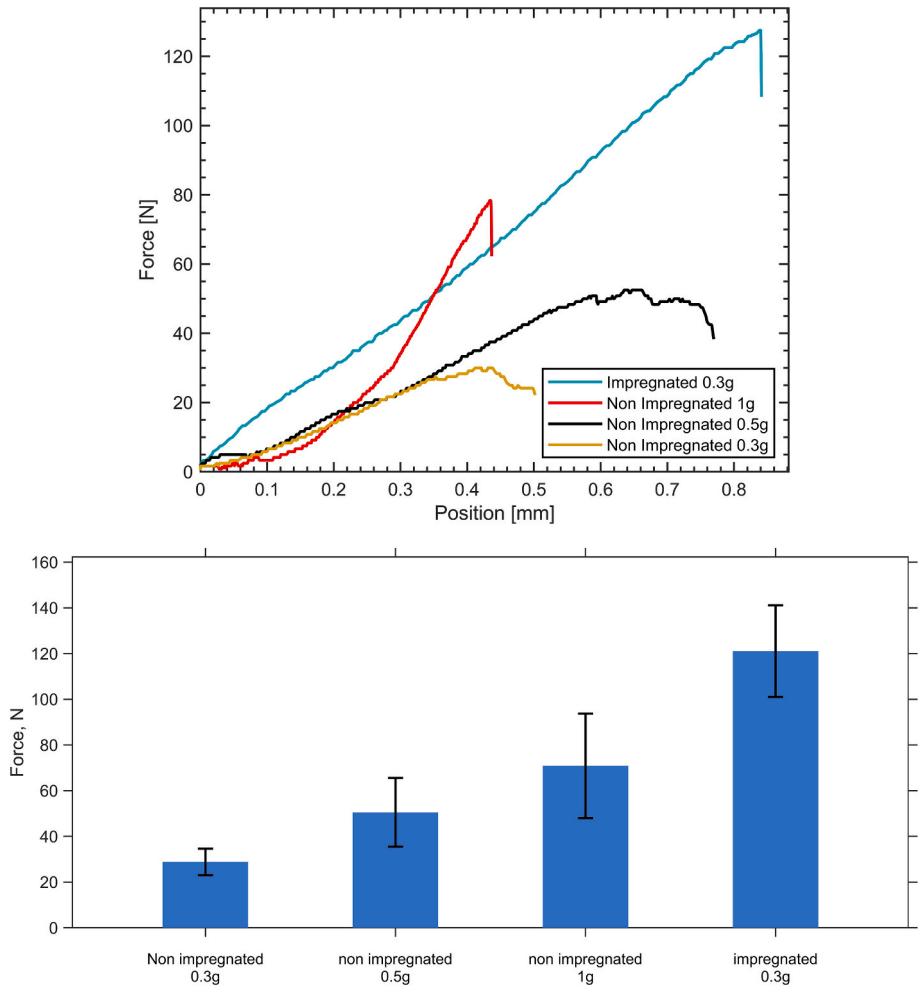

Fig. 5. A) pull-out test results of impregnated and non-impregnated ccf tow, b) the adhesion force of impregnated and non-impregnated ccf tow with different amounts of polymer.

Table 2
Interlayer adhesion test results (number of samples, n = 6).

Parameter	Mean	Standard Deviation	Coefficient of Variation (%)	95% Confidence Interval (CI)	Min-Max
Maximum force (N)	1129.2	124.2	11.0	998.8–1259.5	936.0–1280.0
Shear area, (mm^2)	139.3	7.6	5.5	131.3–147.4	126.0–147.0
Shear strength (MPa)	8.1	0.5	6.6	7.5–8.6	7.4–8.8

with limited specimen-to-specimen scatter. This suggests a high level of production process precision and indicates that sample size is sufficient to provide a reliable conclusion. Based on the plots and statistical data, it can be concluded that the interlayer adhesion between the PLA polymer and the impregnated filament is satisfactory. Moreover, the mMEX additive manufacturing technique proves to be a reproducible manufacturing method for fabrication of composite structures reinforced with continuous fibers.

The failure mode analysis was conducted in accordance with ASTM D5573. Each sample was examined after adhesion testing, and all specimens were found to exhibit adhesive failure. Specifically, the adhesive at the overlapping joint failed while the fibres remained intact. The failure occurred exclusively at the overlap region of the composite specimens, with clean polymer debonding observed after testing. Although all samples demonstrated adhesive failure, a light fiber tear was also observed, particularly at the top part of lower adherend. This phenomenon is related to the production process of SLJ specimens. In general, continuous carbon fiber tow is embedded in the upper portion of the printed composite line, therefore, fibers from top layer of bottom adherend are in direct contact with the polymer of upper adherend. Consequently, a small amount of fiber pull-out or tearing occurs during the separation of the single lap joint. However, this could be considered more as characteristic of the manufacturing method rather than the primary failure mechanism, and finally it is not dominant in the overall samples.

5. Structural analyses

Structural analyses were performed using two NDT methods: SEM and THz spectroscopy. The structural integrity was analysed for samples after manufacturing and after exposure to elevated (from 10℃ to 50℃) or sub-zero (from 10℃ to −50℃) temperatures. The heating and cooling processes were gradual, with a temperature step of 5°C. The tests were performed at a rate of 0.2℃/min and, stabilisation lasted 30 min. The parameters were chosen to ensure stable and uniform thermal transitions. Each seat contained 5 samples, for structural presentation, one

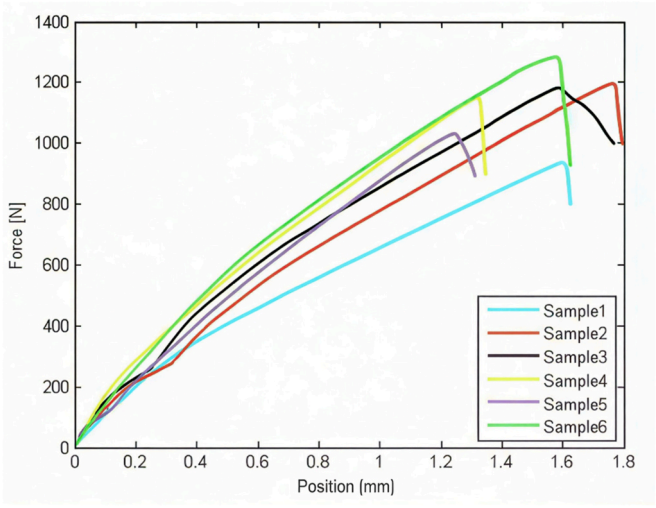

Fig. 6. Plot for the adhesion analysis of a single lap joint composite sample.

representative was chosen as the results achieved during the NDT investigations were similar for all samples from one set. The tests were performed in an environmental chamber, MyDiscovery DM600C (Angelantoni Test Technologies Srl, Italy).

a. Thz spectrometer

In Fig. 7, a comparison of THz signal measured in the chamber (Fig. 3 (b)) for three cases is presented. The first is an empty chamber (denoted as A), as it contains air. The other two are for additively manufactured two-layer CFRP samples with different alignments of reinforced carbon fibres. Due to the carbon fibre content in the unidirectional sample (denoted as CFRP 0/0), a part of the signal is transmitted throughout its whole thickness by polymer or voids. On the contrary, perpendicular alignment of carbon fibres (denoted as CFRP 0/90) results in total attenuation of the signal. Therefore, for the purpose of analysis of adhesive joints in the 3D-printed structures, unidirectional CFRP samples were chosen.

Then, the unidirectional two-layer sample was measured using a scanning unit in reflection mode. In Fig. 8, results are presented in the form of B-scan and C-scans. In the B-scan it is possible to indicate four planes linked with the top and bottom surfaces of the sample, a mid-plane and a metal surface of the table.

Based on this observation, the surfaces were determined using the following equations.

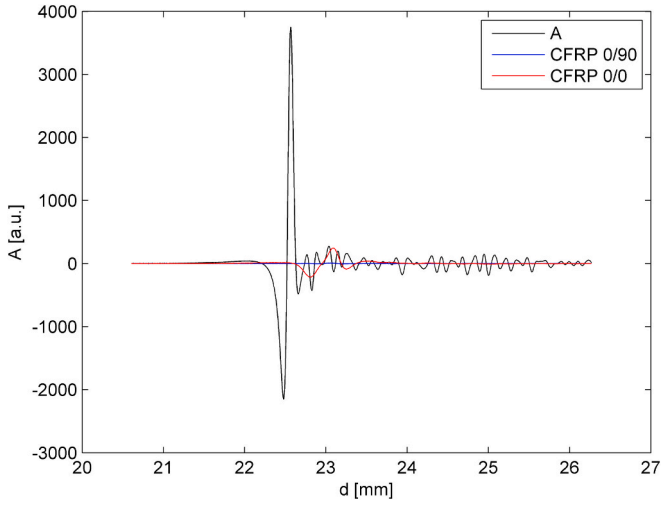

Fig. 7. Comparison of A-scans in transmission mode: A – through air, CFRP 0/90 – through 2-layer sample 0/90, CFRP 0/0 – through 2-layer sample 0/0.

for the top surface.

$T(t,i,j) = min(Z(t,i,j))for t \in \langle 0, A\rangle$ and i = 1,…,i_n; j = 1,…,j_m.

for the bottom surface.

$B(t,i,j) = min(Z(t,i,j))for t \in \langle 0, M\rangle$ and i = 1,…,i_n; j = 1,…,j_m.

for the metal plane.

$M(t,i,j) = min(Z(t,i,j))for t \in \langle T, B\rangle$, and i = 1,…,$i_n$; j = 1,…,$j_m$.

and for the mid-plane.

$P(t,i,j) = max(Z(t,i,j))for t \in \langle 0, M\rangle$ and i = 1,…,i_n; j = 1,…,j_m.

where A and B are arbitrary given numbers determined based on the B-scan.

In the top surface (Fig. 8(b)), the characteristic pattern related to the manufacturing method is visible. It is similar to the top surface of the schematic sample in Fig. 1(b). However, the iCF pattern is not so clear. The reasons are the local roughness of the sample surface on iCF as well as its curvature. Contrary to the schema, the sample thickness varies due to different amounts of polymer between consecutive layers and printed fibres. The mid-surface (Fig. 8(c)) is a polymer layer that was probably created during the printing process from the polymer (P) added to the printing head. It not only filled the emptiness between printed iCFs but, after solidification, created a layer. It is schematically presented in Fig. 1 (c). The quality of the adhesive joint between the polymer P and iCF from both layers is responsible for the material resistance to interlayer delamination during mechanical loading. In the C-scan determined for the bottom surface (Fig. 8(c)), the iCF pattern is more similar to the schematic one. However, it also indicates local non-parallelism of printed iCF and voids occurrence (between 0 and 5 mm in x direction).

The THz results indicate differences in structure between a laminate manufactured using a standard technique (with parallel layers of fibre reinforcement) and AM laminate (with separated fibre reinforcement adhesively joined in one structure).

In the next step, the influence of temperature on the material quality is presented for the set of three samples. Photographs of the three samples are presented in Fig. 9. The THz spectroscopy analyses were performed on the sample after manufacturing, after exposure to elevated (to 50°C) or sub-zero (to −50°C) temperatures. On all samples (Fig. 9), the printing pattern (iCF alignment) is sufficiently visible in the form of differences in flatness of the surfaces. The differences are related to the polymeric component. On the surface of the sample after manufacturing (Fig. 9(a)), the polymer layers are in rows between iCFs. Exposure to elevated temperature results in phase change of the polymer, and the sample surface becomes flatter because the polymer fills the rows between CCF (Fig. 9(b)). Probably, exposure to elevated temperature results in a phase change of the polymer to a semi-liquid state. It was previously reported for a pure PLA sample that the mMEX method reduced characteristic temperatures of the material, probably due to the shorter polymeric chains[33]. A semi-liquid state of polymer is observed for temperatures above its glass transition temperature (Tg) but below its melting temperature (Tm). The Tg of PLA is in the range between 50°C and 70°C, while the maximum temperature during the heating process was 50°C. On the contrary, exposure to sub-zero temperatures results in higher distortion of the sample structure. This probably occurred due to a change in crystallisation of the polymer structure from amorphous to brittle, and a part of it crumbled. There is visible emptiness between CCF.

The samples presented in Fig. 9 were inspected using THz spectroscopy method. B-scan of the three samples with marked top and bottom surfaces, and the metal table is presented in Fig. 10. The sample exposed to elevated temperature is the narrowest. Originally, all samples were manufactured using the same AM method under the same parameters. Most likely, the heating process transformed the polymer form solid to a semi-liquid state. Then the polymer P solidified between carbon fibers without voids. The process influenced the size of the sample in its width direction in a similar way as it is observed in the shrinkage of the mould material.

For the purpose of analysing the internal structure of the CFRP samples, the THz data set was post-processed in a similar way as it was

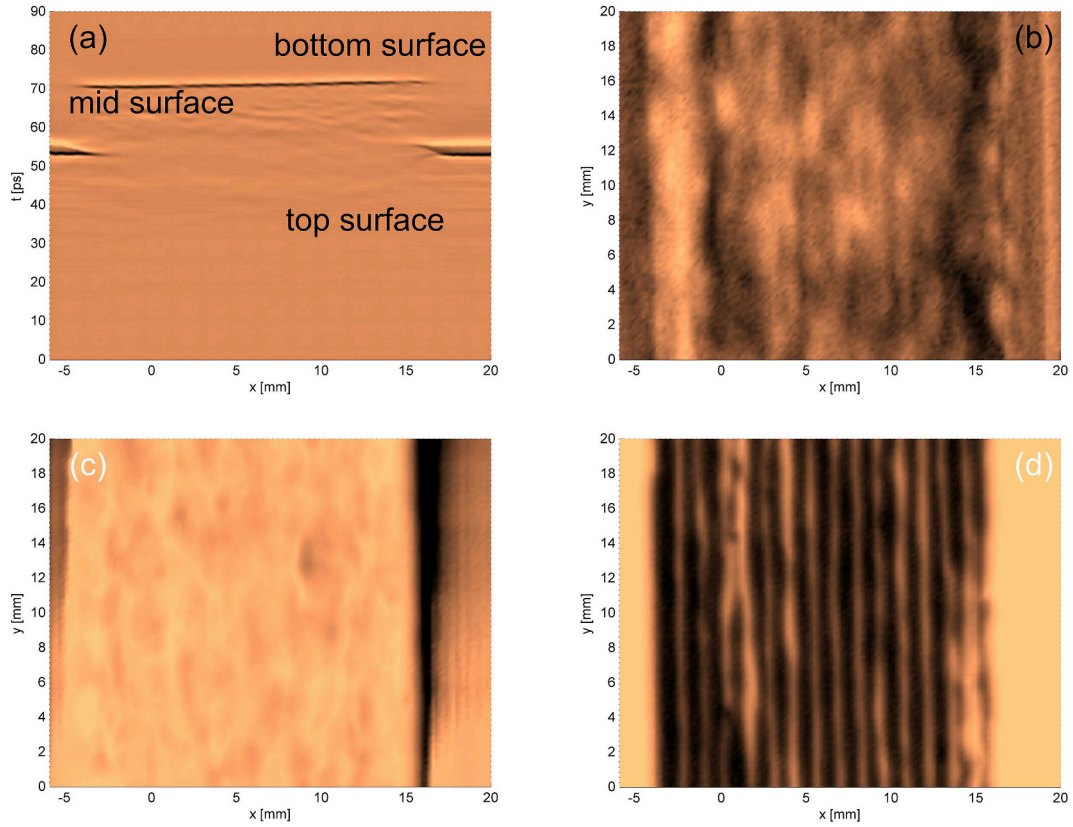

Fig. 8. 2-layer CFRP structure: (a) B-scan, (b) C-scan of top surface, (c) C-scan of mid surface, (d) C-scan of bottom surface.

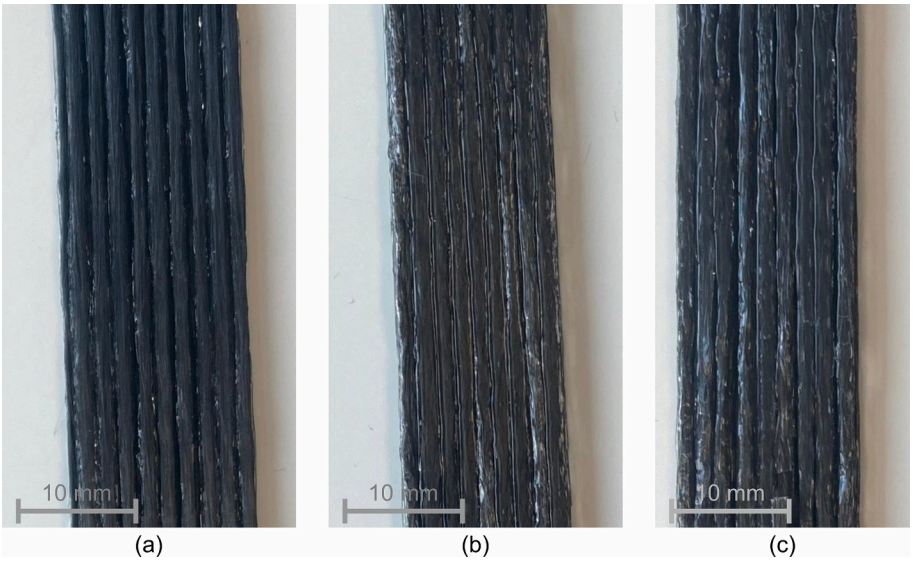

Fig. 9. Photograph of three CFRP samples: (a) after manufacturing, (b) after elevated temperature, (c) after sub-zero temperature.

presented earlier for the two-layer sample. Among the achieved C-scan sets, two were chosen: for the bottom surface (B) and for the metal plate (M). Both visual inspection and SEM analyses presented that temperature influenced the polymer component of the samples. THz spectroscopy can be applied to non-conductive materials only. Therefore, two surfaces were selected that required THz wave transmission throughout the whole thickness of the sample.

C-scans for the bottom surface of the samples are presented in Fig. 11 (a). In all samples, the additively manufactured carbon fibres pattern is clearly visible. In theory, the fibre reinforcement is aligned parallel as intended during the manufacturing process. However, the presence of imperfections results in local curvature of the fibres. In the as-manufactured samples, voids appear as darker areas. An unequal distribution of polymer along the carbon fibre, leads to local variations in the spacing between adjacent fibres. In the samples exposed to sub-zero temperatures, the absence of polymer is observed as bright regions oriented parallel to the carbon fibre bundles. On the contrary, the equality in polymer and fibre distribution is visible in the structure of the sample after the heating process.

C-scans for the metal plate surface of the samples are presented in

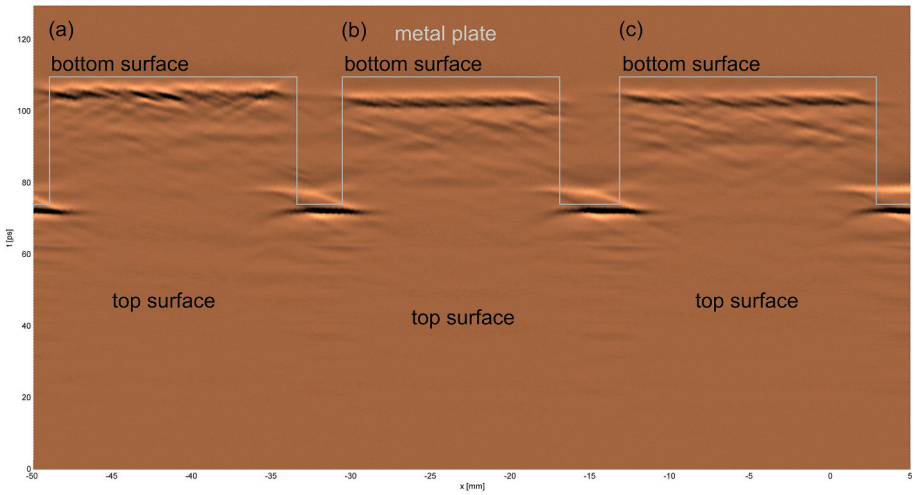

Fig. 10. THz image (B-scan) of three CFRP samples: (a) after manufacturing, (b) after elevated temperature, (c) after sub-zero temperature.

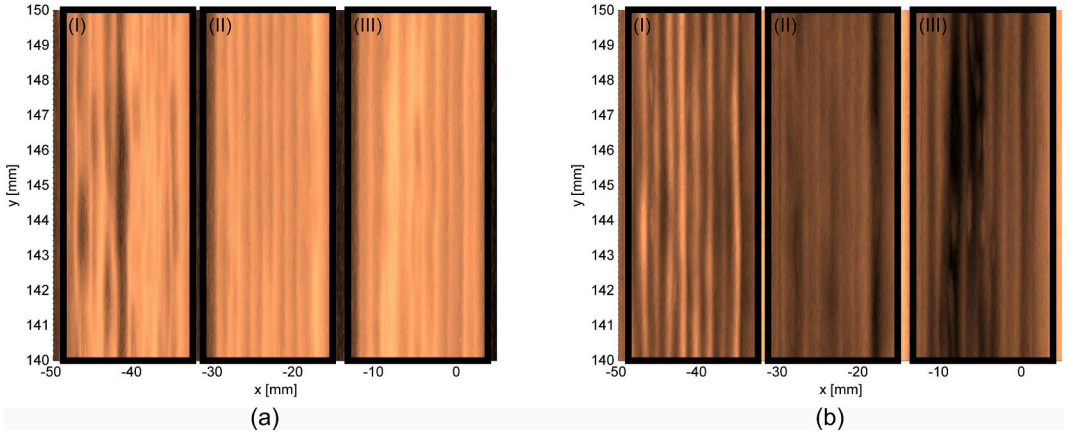

Fig. 11. THz image (C-scan) of three CFRP samples for (a) bottom surface, (b) the metal plate: (I) after manufacturing, (II) after elevated temperature, (III) after sub-zero temperature.

Fig. 11(b). Also in the C-scan, the carbon fibre pattern is visible for all samples. Additionally, the structural integrity differences among the samples are observable. In the sample after manufacturing, the unequal distribution of the polymer is visible as brighter and darker strips. The elevated temperature influence in the form of filling the areas between fibre reinforcement by polymer is visible as an area with a similar colour. However, the darker parts can suggest that damage due to thermal stress occurred. Sub-zero temperatures also influenced the polymer component of the CFRP. The emptiness is in the form of dark areas.

b. SEM analyses

After the more general analyses of the CFRP samples structures related to both components (polymer and fibre), relations between them, and the differences between the assumed (Fig. 1(b)) and the real structures, more detailed SEM analyses were performed.

For more detailed analyses of the structural integrity of the samples, SEM analyses were performed on the samples presented in Fig. 9. They were focused on composite components (carbon fibre and polymer).

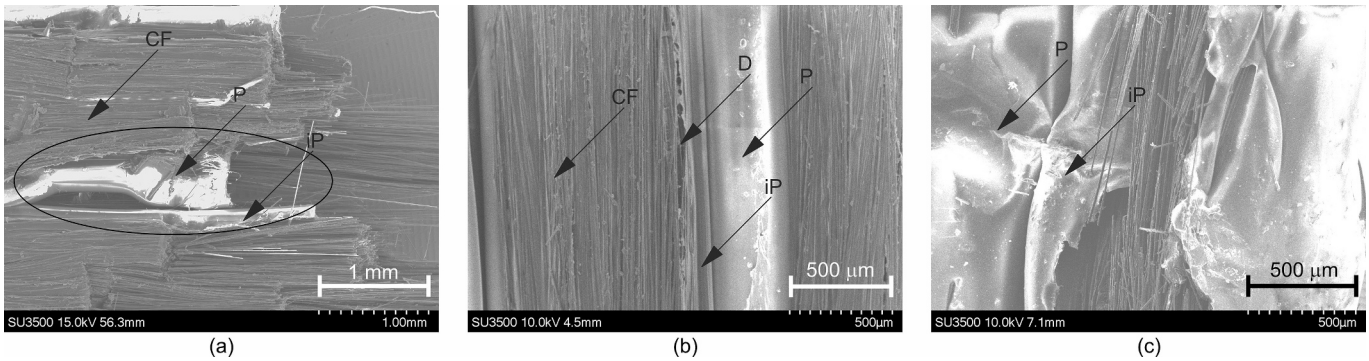

Fig. 12. SEM photographs of CFRP samples presenting material components (carbon fibres and polymer) after: (a) manufacturing, (b) exposure to elevated temperature (from 10℃ to 50℃), (c) exposure to sub-zero temperature (from 10℃ to −50℃); CF – carbon fibre, P – polymer, iP – impregnation polymer, D – damage.

Three SEM photographs are presented in Fig. 12. In the photograph of the sample after manufacturing (Fig. 12(a)), it is possible to distinguish two types of polymer: iP (covering carbon fibre) and P (filling areas between printed iCF lines). It is visible that the pre-impregnation process results in proper adhesion between iP and CF, forming iCF (black spool in Fig. 1(a)). While polymer P added during the AM process does not fill the whole area between carbon fibre bundles, and voids are well visible. The observation confirms that adhesion between P and iP is crucial for the material durability. On the contrary, in the photograph of the sample after heating (Fig. 9(b)), the whole area between carbon fibres is filled by the polymer, resulting in a structure with parallel black and white strips with thickness related to the type of carbon fibre bundles (3 K) and rows between 3D-printed iCF. The heating process influenced the polymer P shape, but the boundary between iP and P is still visible. However, it seems that the heating process negatively influenced the adhesive boundary between CF and iP in iCF, as damage (D) can be observed. Based on the achieved results, it seems that heat treatment can increase the quality of the material. However, more analyses are required to appropriately design the heat treatment process. Sub-zero temperature influenced the structure of CFRP (Fig. 9(c)). Two versions of polymer (P and iP) are visible. Additionally, there is no good connection between them. The adhesive joints between them are only local. In the other parts, voids are visible. The SEM observations are in good agreement with the visual inspection presented before.

The SEM micrograph of the as-manufactured specimen shows multiple, co-localized failure modes. Fibre pull-out, evident as long, exposed

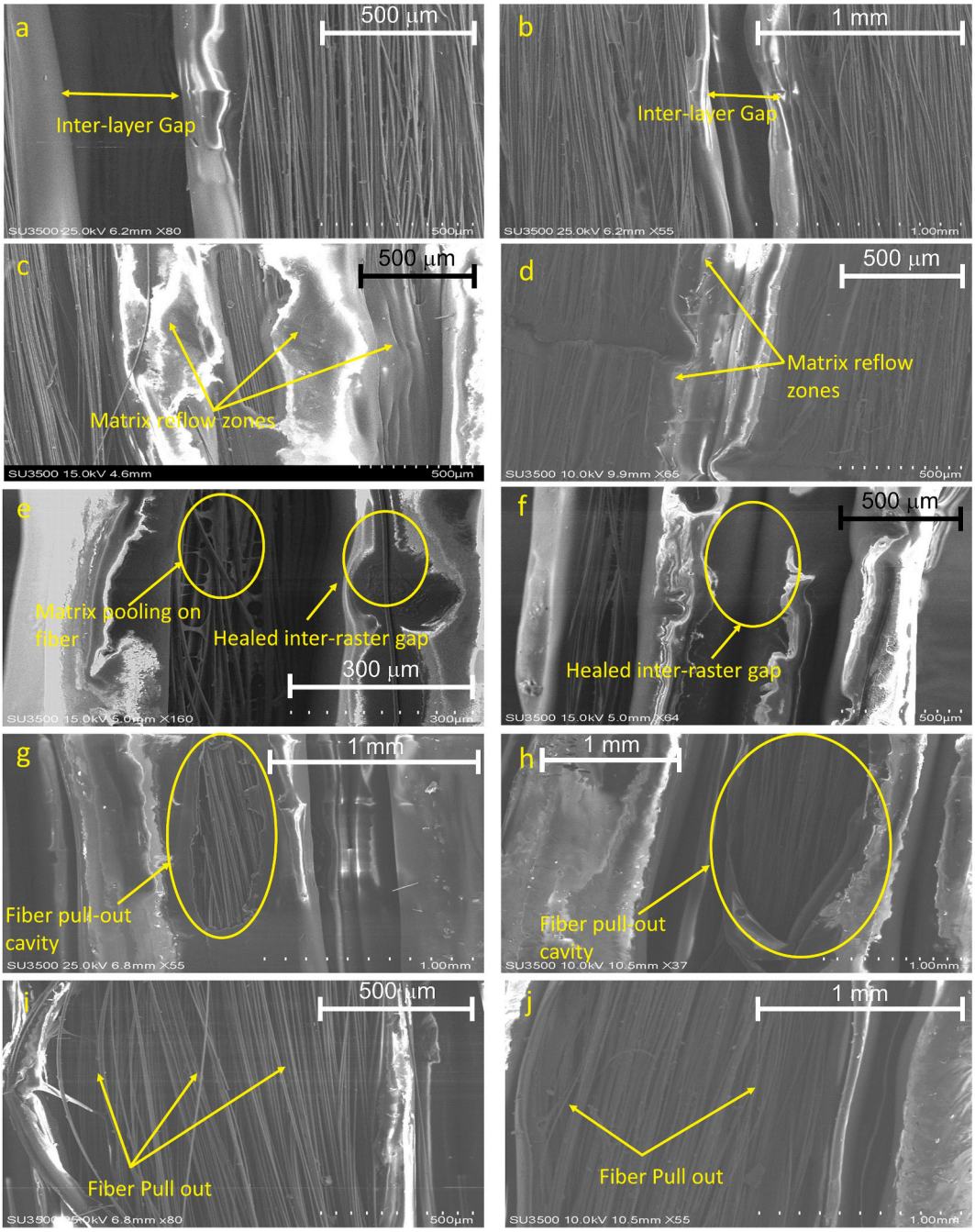

Fig. 13. SEM images: (a), (b) as manufactured samples showing gaps between adjacent layers, (c), (d) reflow of the matrix material on the fiber due to thermal exposure, (e), (f) improved adhesion visible from the healed inter-raster gap and matrix pooling on fibre bundle, (g), (h) the fracture surface show large, elongated cavity showing carbon fibre bundle pulled from the matrix, (i), (j) closer view of the pull-out region revealing absence of polymer films.

carbon filaments with the absence of residual PLA, shows weak fibre matrix bonding. The gaps between the printed layers further indicate incomplete fusion (Fig. 13(a),(b)). Fig. 12(a) shows smooth, mirror-like facets at the boundary where the thin PLA "skin" impregnating the fibre bundle has cleanly separated from the bulk PLA matrix. Despite identical polymer chemistry, the impregnated PLA did not molecularly fuse with the printed matrix. The absence of polymer "bridges" and the presence of fine cracks along these interfaces implicate differences in local cooling rates, shear histories, or crystallinity as one of the root causes.

SEM examination of samples subjected to elevated temperature revealed microstructural changes that correlate with their enhanced mechanical performance. The voids and gaps at the interfaces between adjacent rasters were narrowed or even eliminated in some regions, reflecting a localized reflow of the PLA matrix due to thermal exposure (Fig. 13(c),(d)). In Fig. 13(e),(f), softened PLA has flowed into the inter-raster gaps and partially healed the area, enabling it to withstand higher loads. The matrix appears to have pooled and resolidified around the fibre bundle, demonstrating enhanced wetting and fibre-matrix bonding. Although fibre pull-out still occurred, leading to the specimen's ultimate failure under tensile load, the specimen exhibited increased strength. This improvement can be attributed to thermal exposure, which enhanced adhesion by better impregnating the polymer matrix and strengthening the fibre-polymer interface. These SEM observations demonstrate that a controlled post-printing thermal exposure markedly enhances both inter-raster and fibre matrix adhesion in mMEX fabricated PLA- CFRP composites, thereby extending their suitability to high strength structural applications. This thermal reflow mechanism, where post-processing at elevated temperatures promotes polymer redistribution and void elimination is consistent with the enhanced interfacial bonding reported in co-cured CFRP joints subjected to post-curing treatment, where improved matrix-fibre contact area leads to stronger mechanical interlock and diffusion bonding at the interface [34].

To understand the microstructural behaviour and mechanical characteristics, the same specimens were exposed to sub-zero temperatures. Fig. 13(g),(h) reveals a post-fracture morphology of the specimen following the exposure to sub-zero temperature. The elongated cavity shows where a carbon fibre bundle was exposed from the polymer matrix. It indicates the fibre–matrix interface failed in shear rather than the fibre fracturing or the matrix plastically deforming. The fibre pull-out from the closer look in Fig. 13(i),(j) provides direct evidence that interfacial shear strength was exceeded under loading resulting in adhesive debonding rather than cohesive failure of the either constituent.

Surrounding the pull-out zone, the PLA matrix exhibits faceted cleavage patterns with negligible fibrillary stretching. The absence of drawn-out fibre strand demonstrates brittle matrix fracture, a behaviour consistent with embrittlement induced by cryogenic exposure. The sharply demarcated cavity and the lack of PLA residues on the fibre surfaces further confirm that poor adhesion at the fibre–matrix interface led to the failure. The sub-zero temperature exposure not only embrittled the PLA but also weakened interfacial adhesion and as a result under tensile stress the composite failed predominantly by fibre pull-out and interfacial separation rather than by fibre breakage or matrix yielding.

6. Conclusion

Structural integrity remains a concern in CFRP structures due to the different mechanical, chemical, and physical properties of the constituent fibre and polymer materials. In laminates manufactured using additive manufacturing (AM) methods, where no additional pressure or loading is applied, adhesion between components plays a vital role in determining overall material strength. In this study, the NDT method (THz spectroscopy) was employed alongside tensile testing to evaluate samples fabricated using the mMEX method. Initial analyses focused on the adhesion between carbon fibre and polymer, and pull-out tests confirmed that pre-impregnation of the carbon fibre was essential. After employing the mMEX (with modified print head) manufacturing method and the incorporation of the impregnation process, two distinct polymer types were identified within the manufactured material: the polymer applied during impregnation (iP) and the polymer introduced during the AM process (P). Despite both being PLA, these polymer types exhibited distinctly different behaviours, and boundaries between them were identifiable across all analysed samples. For a more investigation of structural integrity, SEM was performed on samples following tensile testing and temperature exposure, giving a clear distinction between the two polymer types. Upon exposure to elevated and sub-zero temperatures, the quality of adhesion between iP and P proved crucial in determining the structural integrity of the specimens. Post-processing at elevated temperatures significantly improved adhesive joint quality, eliminating voids as polymer P filled all inter-fibre regions; however, excessively high process temperatures likely induced contraction during PLA solidification, generating compressive stresses at the carbon fibre/iP boundary and causing localised damage.

CRediT authorship contribution statement

Magdalena Mieloszyk: Writing – original draft, Visualization, Supervision, Project administration, Methodology, Investigation, Funding acquisition, Formal analysis, Conceptualization. **Marius Rimasauskas:** Writing – original draft, Validation, Supervision, Methodology, Investigation, Formal analysis, Conceptualization. **Suvam Bhadra:** Writing – original draft, Visualization, Validation, Investigation, Formal analysis. **Muhammad Abuzar Khan:** Writing – original draft, Visualization, Validation, Investigation, Formal analysis.

Declaration of competing interest

The authors declare that they have no known competing financial interests or personal relationships that could have appeared to influence the work reported in this paper.

Acknowledgment

The research was partially supported by the project entitled: Degradation processes of mechanically loaded structures in hydrogen environment (2022/45/B/ST8/03494) granted by National Science Centre in Poland, doctoral scholarship of Mr Muhammad Abuzar Khan is financed by STER mTSDPAN project (BPI/STE/2023/1/00008) granted by the Polish National Agency for Academic Exchange.

Computations were carried out using the computers of Centre of Informatics Tricity Academic Supercomputer & Network.

Data availability

Data will be made available on request.

References

[1] K. Yu, M.L. Dunn, H. Jerry Qi, et al., Recent advances in design optimization and additive manufacturing of composites: from enhanced mechanical properties to innovative functionalities. npj, Adv. Manuf. 2 (2025) 26.
[2] C. Dong, I.J. Davies, Mechanical properties of continuous glass fibre-reinforced composites made by material extrusion, Prog. Addit. Manuf. 9 (2024) 2131–2141.
[3] C. Kousiatza, D. Karalekas, In-situ monitoring of strain and temperature distributions during fused deposition modeling process, Mater. Des. 97 (2016) 400–406.
[4] M. Rimašauskas, T. Kuncius, R. Rimašauskienė, Processing of carbon fiber for 3D printed continuous composite structures, Mater. Manuf. Process. 34 (13) (2019) 1528–1536.
[5] K.I. Ismail, T.C. Yap, R. Ahmed, 3d-printed fiber-reinforced polymer composites by fused deposition modelling (fdm): fiber length and fiber implementation techniques, Polymers 14 (21) (2022) 4659.
[6] E.C. Botelho, L.C. Pardini, M.C. Rezende, Hygrothermal effects on the shear properties of carbon fiber/epoxy composites, J. Mater. Sci. 41 (2006) 7111–7118.

[7] E.S. Romero, E. Barocio, R.W. Trice, Evaluating Extrusion Deposited Additively Manufactured Fiber- Reinforced Thermoplastic Polymers as Carbon/Carbon Preforms, Appl. Compos. Mater. 31 (2024) 399–419.
[8] C. Pascual-González, P.S. Martín, I. Lizarralde, A. Fernández, A. León, C. Lopes, J. Fernández-Blázquez, Post-processing effects on microstructure, interlaminar and thermal properties of 3D printed continuous carbon fibre composites, Compos. B Eng. 210 (2021) 108652.
[9] M.T. Aranda, L. Tavara, J. Reinoso, P.P. Camanho, Single lap joint (SLJ) fracture assessment of 3D printing composite parts using structured and flat interface definitions: Experimental and numerical study, Compos. Struct. 355 (2025) 118788.
[10] B.M. Gackowski, M. Sharma, X.Q. Koh, D.H.L. Seng, D. Verma, V. Raveenkumar, S. Idapalapati, Surface engineering of carbon nanotube-carbon fiber networks for enhanced strength in additive manufacturing of nylon composites, Compos. A Appl. Sci. Manuf. 186 (2024) 108383.
[11] M. Handwerker, J. Wellnitz, H. Marzbani, U. Tetzlaff, Pressure and heat treatment of continuous fibre reinforced thermoplastics produced by fused filament fabrication, Prog. Addit. Manuf. 8 (2022) 1–18.
[12] M. Eftekhari, A. Fatemi, Tensile behavior of thermoplastic composites including temperature, moisture, and hygrothermal effects, Polym. Test. 51 (2016) 151–164.
[13] Eslami, S., Taheri-Behrooz, F., Taheri, F., 2012. Effects of aging temperature on moisture absorption of perforated GFRP. Advances in Materials Science and Engineering 2012.
[14] A.K. Shrivastava, M. Nazir Hussain, Effect of low temperature on mechanical properties of bidirectional glass fiber composites, J. Compos. Mater. 42 (22) (2008) 2407–2432.
[15] S.P. Zaoutsos, M.C. Zilidou, Influence of extreme low temperature conditions on the dynamic mechanical properties of carbon fiber reinforced polymers, IOP Conf. Ser.: Mater. Sci. Eng. 276 (2017) 012024.
[16] Y. Nawab, F. Jacquemin, P. Casari, N. Boyard, Y. Borjon-Piron, V. Sobotka, Study of variation of thermal expansion coefficients in carbon/epoxy laminated composite plates, Composites Part B 50 (2013) 144–149.
[17] L. Liu, M. Du, F. Liu, Recent advances in interface microscopic characterization of carbon fiber-reinforced polymer composites, Front. Mater. 10 (2023).
[18] V. Jain, A. Bisht, S. Jaiswal, K. Dasgupta, D. Lahiri, Assessment of interfacial interaction in graphene nanoplatelets and carbon Fiber-Reinforced epoxy matrix multiscale composites and its effect on mechanical behavior, J. Mater. Eng. Perform. 30 (12) (2021) 8913–8925.
[19] C.G. Harris, N.J.S. Jursik, W.E. Rochefort, T.W. Walker, Additive manufacturing with soft TPU – adhesion strength in multimaterial flexible joints, Frontiers in Mechanical Engineering 5 (2019).
[20] Y.A. Sütcüler, G.J.P. Bex, C.A. Stupp, M. Kodal, A.T.T. Cate, G. Özkoç, Lab-scale manufacturing of thermoplastic matrix-continuous carbon fiber filaments for additive manufacturing: Melt impregnation, properties of the filaments and its printed composites, Polym. Compos. (2024).
[21] D. Mittleman, Sensing with Terahertz Radiation, Vol. 85, Springer, 2013.
[22] Y. Zhang, J. Han, D. Wang, X. Li, T. Qiu, H. Chen, et al., Application of THz time-domain spectroscopy to diagnose gastric cancer tissues in surgical resected specimens, J Infrared Millim Terahertz Waves 42 (2021) 802–812.
[23] M. Peccianti, R. Fastampa, A.M. Conte, O. Pulci, C. Violante, J. Łojewska, et al., Terahertz absorption by cellulose: Application to ancient paper artifacts, Phys. Rev. Appl 7 (6) (2017) 064019.
[24] C.-H. Ryu, S.-H. Park, D.-H. Kim, K.-Y. Jhang, H.-S. Kim, Nondestructive evaluation of hidden multi-delamination in a glass-fiber-reinforced plastic composite using terahertz spectroscopy, Compos. Struct. 156 (2016) 338–347.
[25] M. Mieloszyk, K. Majewska, W. Ostachowicz, Application of THz spectroscopy for localisation of fibre optics embedded into glass fibre reinforced composite, Compos. Struct. 209 (2019) 548–560.
[26] X. Lu, Y. Shen, T. Xu, H. Sun, L. Zhu, J. Zhang, et al., Accurate detection of porosity in glass fiber reinforced polymers by terahertz spectroscopy, Composites, Part B, Eng 242 (2022) 110058.
[27] M. Mieloszyk, P. Madejski, S. Wroński, I.I. Muna, Structural analyses of additively manufactured carbon fiber reinforced polymer with embedded fiber optic using THz spectroscopy and micro-computed tomography, Opt. Lasers Eng. 193 (2025) 109086.
[28] O.C. Zehni, Y. Malevich, A. Kandemir, C. Valles, M.A. Bissett, C. Kocabas, I. A. Kinloch, Carbon contrast agents for terahertz spectroscopic NDT of impacted glass fibre reinforced plastics, Compos. Sci. Technol. 257 (2024) 110795.
[29] M. Strąg, W. Świderski, Non-destructive inspection of military-designated composite materials with the use of Terahertz imaging, Compos. Struct. 306 (2023) 116588.
[30] D.H. Han, Inner defect detection of glass fiber reinforced polymer sandwich panel using pulsed terahertz imaging based on smoothing and derivative, NDT & E International 138 (2023) 102862.
[31] F. Ospald, W. Zouaghi, R. Beigang, C. Matheis, J. Jonuscheit, B. Recur, et al., Aeronautics composite material inspection with a terahertz time-domain spectroscopy system, Opt. Eng. 53 (3) (2014) 031208.
[32] N. Karpowicz, D. Dawes, M.J. Perry, X.-C. Zhang, Fire damage on carbon fiber materials characterized by THz waves, Int. J. High Speed Electron. Syst. 17 (02) (2007) 213–224.
[33] I.I. Muna, M. Mieloszyk, Temperature influence on additive manufactured carbon fiber reinforced polymer composites, Materials 14 (21) (2021) 6413.
[34] N. Karthikeyan, J. Naveen, V.S. Hiremath, Investigating the synergistic effects of geometric (interleaved lamina) and adhesive modifications on the shear behavior of co-cured CFRP composite joint: Prediction and optimization using statistical and deep learning approach, Results Eng. 26 (2025) 105451.